Development of sodium hybrid quasi-solid electrolytes based on porous NASICON and ionic liquids

C.S. Martínez-Cisneros [a], B. Pandit [a], C. Antonelli [b], J.Y. Sanchez [a,c], B. Levenfeld [a], A. Varez [a,*]

[a] *Materials Science and Engineering Department, University Carlos III of Madrid, Spain*
[b] *Institut Européen des Membranes (IEM), UMR-5635, Université de Montpellier, ENSCM, CNRS, Place Eugène Bataillon, 34095, Montpellier cedex 5, France*
[c] *Univ. Grenoble Alpes, Univ. Savoie Mont Blanc, CNRS, Grenoble INP, LEPMI, 38 000, Grenoble, France*

ARTICLE INFO

ABSTRACT

Lithium-ion batteries are currently the alternative of choice to overcome the increasing demand of energy. However, besides the scarcity of lithium and limited geolocation, it is believed that such batteries have already reached their maximum maturity. Sodium batteries emerge as an alternative to produce the new, so called, post-lithium batteries. In this study, we explore (i) the effect of sodium content and sintering temperature in solid electrolytes based in NASICON-type compounds and (ii) the use of two methodologies to obtain porous NASICON samples: application of natural substances and organic materials as pore-formers and freeze casting. The main purpose is the attainment of hybrid quasi-solid state electrolytes, with enhanced room temperature conductivity, based on porous ceramic electrolyte layers infiltrated with ionic liquids. Using this approach, porous samples with different microstructure and porous morphology and distribution were achieved, providing an enhancement in conductivity (ranging from 0.45 to 0.96 mS cm^{-1} at 30 °C) of one order of magnitude for infiltrated samples respect to pore-free samples. According to these results the porous NASICON might be considered as a functional macroporous inorganic separator that can act as a Na$^+$ reservoir.

1. Introduction

The transition to less carbon-dependent energy systems demands increasingly efficient and sustainable systems, in accordance with clean renewable energy sources, to regulate intermittent energy demands [1, 2]. Rechargeable batteries play an important role in storing energy from renewable sources, as they can be used on demand. Beyond costs per kWh and performances, safety and ores scarcity remain as major concerns in batteries. This contribution addresses both concerns as 1) despite unmatched energy density, the safety of large capacity lithium batteries, due both to their high energy content and to their flammable organic liquid solvents [3], remains questionable, and 2) the scarcity in lithium ores is a mid to long term issue that compromises their use to store renewable electricity. Due to sodium high abundance, thus low cost, sodium batteries (NaB) are considered one of the most promising alternatives to LiB. Additionally, NaB benefit from long-term academic and industrial knowledge regarding their components, i.e. electrodes and electrolytes, and their systems, e.g. ZEBRA battery. Even though Na capacities (1.16 Ah.g^{-1} and 1.12 Ah.cm^{-3}) are fairly modest when compared to Li, Mg and Ca, NaB are probably the technology closest to

reach the industrial development. Indeed, due to similar physical/chemical properties, NaB can take advantage of the knowledge on LiB [4]. Despite NaB are probably unsuitable, in their current state, for their automotive implementation (limited energy density), stationary energy storage is expected to be their one significant application (cost advantage [5,6]).

Regarding safety concerns, among the strategies to improve battery safety, those discarding low Flash Point components are probably the best ones. Thus, LiB based on solvent-free polymer electrolytes used both as electrolyte and as binder of positive electrodes have been demonstrated, at the 10 Ah scale [7]. To minimize the flammability of batteries, one option is to incorporate a ceramic or glass component as electrolyte, as thick binder-free electrode [8] or as both [9].

In terms of safety, all solid state sodium batteries (ASSSB) emerge as a promising next generation with enhanced thermal and electrochemical stability, lower flammability and improved durability [10,11]. Solid electrolytes are a crucial part in ASSSB, providing a mechanical barrier that might hinder dendrite growth, providing a wider electrochemical window, which results in higher volumetric energy density when compared to those batteries based on liquid electrolytes [12,13].

Nowadays, the most widely used Na-based solid-state electrolytes are based on Na-β"-Al$_2$O$_3$, NASICON, and Na$_3$PS$_4$ glass-ceramic sulfides [14–16]. NASICON compounds, Na$_{1+x}$Zr$_2$P$_{3-x}$Si$_x$O$_{12}$ (0 ≤ x ≤ 3), unlike Na-β"-Al$_2$O$_3$, have a three dimensional structure with suitable tunnels for Na$^+$ migration, which at high temperature renders ionic conductivity values, comparable to those exhibited by liquid electrolytes [17,18]. NASICON can crystallize in a rhombohedral structure when PO$_4$ or SiO$_4$ tetrahedral shares corners with ZrO$_6$ octahedral, which favors ionic conductivity. Nevertheless, when x ranges between 1.8 and 2.2, a monoclinic distortion is observed, which could facilitate sodium ions migration [19,20], achieving the highest ionic conductivity for x = 2, with values ranging up to 10^{-1} S cm^{-1} at 300 °C and 10^{-4} S cm^{-1} at room temperature [21,17]. The high ionic conductivity, wide electrochemical window and high thermal and chemical stability have mainly promoted the application of NASICON compounds as solid electrolytes for NaB [22–26]. According to the literature, the study of the electrochemical stability window highly depends on the method used to evaluate it. Regarding NASICON type electrolytes, a wide electrochemical window is typically reported when applying cyclic voltammetry (~6 V). However, given the restricted effective electrode/electrolyte contact area, lower values have been experimentally obtained by alternative techniques, including in situ X-ray Photoelectron Spectroscopy (XPS) and Energy-Dispersive X-ray Spectroscopy (EDS) [27].

In case of NASICON compounds, the high sintering temperatures and long times produce the volatilization of some constituents (mainly P$_2$O$_5$ and Na$_2$O) and the subsequent segregation of zirconia at the grain boundaries, increasing the grain boundary resistance and, consequently, the total resistance of the ceramic electrolyte. Moreover, the use of ceramic electrolytes punishing the electrolyte-electrode interface, limits the applications of these materials. To overcome this hurdle, several strategies have been proposed: (1) the use of new sintering process such as Spark Plasma Sintering (SPS) [28]; (2) the use of low temperature synthesis methods [29]; (3) the addition of an excess of Na respect to the stoichiometric to compensate its volatile loss during reaction and sintering [30,31]; (4) the rare-earth element doping of NASICON increasing the density of solid-state electrolytes [32,33]; (5) the use of ion conductive polymers to obtain hybrid solid-state electrolytes [34,35], which leads to enhanced ionic conductivity [36,37] and a superior electrode-electrolyte interface [38,39]. In this direction, we have recently carried out a study of NASICON powders coated with N-butyl-N-methylpyrrolidinium bis(trifluoromethanesulfonyl)imide ionic liquid but, in the tested conditions, no synergic effect on the resulting hybrid electrolyte was found [40]. Ionic liquids present a wide electrochemical stability window (3–6 V) [41], which is usually determined in the same way as for liquid electrolytes. In the particular case of ILs with the amide anion, [N(CF$_3$SO$_2$)$_2$]$^-$, they are oxidized at relatively high anodic potentials, which implies the broad stability of this kind of ILs. The most common stability is around 4.5 V [42].

In this work, a systematic study of the effect of sintering temperature and of sodium excess on the microstructure and electrical properties of NASICON solid electrolytes is performed, with the stoichiometric formula: Na$_3$Zr$_{1.84}$Y$_{0.16}$Si$_2$PO$_{12}$ [33]. The best sintering conditions and sodium concentration were used for the development of hybrid quasi-solid electrolytes based on porous NASICON ceramic layers infiltrated with ionic liquids. To produce porous NASICON layers, two methodologies were applied: i) the use of organic materials as pore-formers (rice starch, cornstarch, potato maltodextrin and PMMA (poly-methyl methacrylate)); and ii) the use of freeze casting. The microstructure, homogeneity and mechanical properties of the prepared samples have been investigated by scanning electron microscopy (SEM), X-ray diffraction and Vickers microhardness. Subsequently, porous ceramic NASICON layers were infiltrated with a solution of a commercial ionic liquid (1-Butyl-1-Methylpyrrolidium (trifluoromethanesulfonyl)imide-Pyr0408a) and NaTFSI. The effectiveness of this immersion process is studied in terms of wettability by means of contact angle measurements. Finally, the hybrid electrolytes were characterized by impedance spectroscopy.

2. Experimental

2.1. Samples preparation

According to the literature [21,17], the "bare sample" was prepared by a conventional solid state reaction process with the composition Na$_3$Zr$_{1.84}$Y$_{0.16}$Si$_2$PO$_{12}$. For this purpose, the stoichiometric amounts of the following reagents as precursors were used: Na$_2$CO$_3$ (Merk), (NH$_4$)H$_2$PO$_4$ (Merk), SiO$_2$ (Merk) and fully stabilized zirconia powder (8 mol % YSZ from Tosoh). To investigate the effect of sodium-excess on the material properties as well as its loss during the sintering process due to possible evaporation, some compositions including an excess in sodium (10 wt.% and 20 wt.% regarding the stoichiometric composition), were prepared.

NASICON powders were synthesized based on a procedure reported by [30], with slight modifications. In particular, powders were ball-milled in wet (ethanol) for 24 h at 350 rpm in zirconia jars using 5 mm diameter balls of the same material. After removing ethanol (heating at 60 °C overnight), the ball-milled mixtures were preheated at 500 °C for 4 h followed by 800 °C for 4 h and calcinated at 1100 °C for 4 h in air atmosphere. Both thermal processes were performed in zirconia crucibles to prevent any reaction of powders with the container and subsequently sample contamination. Pore-free samples were obtained by uniaxial pressing by applying 220 MPa during 5 min (pellets: 13 mm diameter; ~ 1 mm thick). The sintering process took place between 1100 and 1200 °C, covering samples with powders of the same composition to reduce the evaporation of sodium and/or phosphorus.

To obtain porous samples, two approaches were applied: i) the use of natural substances (ecological and environmentally friendly) and organic materials as pore-formers and ii) the use of freeze-casting (green approach). In both cases, samples were prepared using the stoichiometric composition corresponding to bare samples (Na$_3$Zr$_{1.84}$Y$_{0.16}$Si$_2$PO$_{12}$), no Na-excess.

2.1.1. Samples prepared by using pore-formers

To produce porous samples by using this approach, different porous formers were tried: rice starch, cornstarch, potato maltodextrin and PMMA (poly(methyl methacrylate)). In order to produce different degree of porosity, two volume fractions of pore formers were used: 10 vol.% and 20 vol.%. Controlled amounts of NASICON and pore-formers powders were mixed using acetone in an agate mortar for more than 10 min. Samples were uniaxially pressed at 220 MPa during 5 min to obtain pellets 13 mm diameter. Pellet samples were sintered, according to the optimization process for sintering, at 1200 °C during 10 h in air atmosphere.

2.1.2. Samples prepared by freeze-casting

For this approach, aqueous slurries were prepared on the basis of those methodologies applied to TiO$_2$ [43], SiC [44] and Al$_2$O$_3$ [45,46]. In summary, butyl phosphate and polyvinyl alcohol (PVA) were used as dispersant and as binder, respectively, to improve green strength for easy handling. NASICON slurries were prepared at 30 vol.%, 40 vol.% and 50 vol.%, respectively. Prior to the NASICON slurry preparation, a 3% PVA solution was prepared in deionized water using a magnetic stirrer at 80 °C for 4 h. The PVA solution was then mixed with the NASICON powder and 3 wt.% of dispersant using a magnetic stirrer during 48 h. Table 1 summarizes the slurries composition. The so obtained slurries were degassed under vacuum for 10 min, poured into small cylindrical silicon molds (10 mm diameter and 15 mm high) and frozen by using a non-contact support adapted to a liquid nitrogen container, so directional freezing was achieved. After completely frozen, molds containing samples were placed in a freeze dryer, where water was sublimated at −50 °C under vacuum during 24 h. Due to sublimation of the ice crystal, porous green samples were obtained. After

Table 1

Composition of the slurries.

Role	Component	Amount	
Inorganic Powder	NASICON	3.2 g	
Dispersant	Butyl phosphate	0.096 g	
		30 vol.%	2.3 mL
Binder/Solvent	3% PVA solution	40 vol.%	1.5 mL
		50 vol.%	1 mL

lyophilization, cylinder-shaped samples were carefully stripped out from the molds, placed on zirconia baskets and quickly transferred to the furnace where they were sintered, according to the optimization process for sintering temperature, at 1200 °C during 10 h in air atmosphere.

2.1.3. Preparation of the hybrid solid electrolyte (HSE)

A solution of 1-Butyl-1-Methylpyrrolidium bis(trifluoromethanesulfonyl)imide (Pyr0408a) and NaTFSI (90:10) was used to infiltrate porous layers during this study. To provide a uniform ion-blocking contact for electrical characterization, prior to infiltration, sintered pellets were gold coated on the top and the bottom surfaces by using a gold ink. Infiltration of samples was performed in a glove box by immersing samples in the ionic liquid solution while applying vacuum during 10 min. Using this methodology, the ionic liquid solution was forced to penetrate through the porous structure, reaching a weight ratio of about 17 % in all cases.

2.2. Characterization techniques

2.2.1. Scanning electron microscopy (SEM)

Microstructure of porous samples was studied by using a FEI TENEO FEG-Scanning Electron Microscope operating at an accelerated voltage 0.2−30 kV. The distribution of sodium through the cross-sectional area of the electrolytes was studied by X-ray mapping, which involves the creation of multiple elemental maps performed at 10 kV and 0.8 nA using the EDAX TEAM™ EDS Analysis System.

2.2.2. X-Ray diffraction

X-Ray diffraction (XRD) experiments were carried out using a Philips X'PERT MPD diffractometer (Cu Kα radiation) operating at 40 kV and 40 mA. The XRD patterns were recorded over a 2θ range of 5−80° using a step scan of 0.02 ° and a counting time of 1 s per step.

2.2.3. Vickers micro-hardness

Mechanical properties were characterized by using Vickers micro-hardness. Previous to the test, samples were polished using silicon carbide abrasive grinding paper (220, 320, 500, 650 and 1000 grit-size). Hardness measurements were performed using a microhardness tester Zwick/Roell by applying a load of 0.5 kgf during 10 s. To favor reproducibility, ten measurements were taken at each surface and the mean value was given, discarding those values that deviated more than 2 times the standard deviation.

2.2.4. Contact angle

To study wettability of porous samples regarding the ionic liquid solution (*1-Butyl-1-Methylpyrrolidium bis(trifuoromethanesulfonyl)imide* - Pyr0408a), the physical contact angle was measured at room temperature using an OCA 15plus contact angle system (Neurtek Instruments, Spain). For this purpose, 1.5 μl drops were disposed on the pellets surface.

2.2.5. Density measurements of samples

Porous samples were characterized in terms of density through the Archimedes method by using a density kit (balance Sartorius CP225D). For this purpose, samples were covered with a thick layer of varnish (density = 0.8 g/cm^3) and immersed into deionized water. Using this

approach, the apparent density was estimated according to:

$$\rho = \frac{w_1}{\frac{w_2 - w_3}{\rho_{water}} + \frac{w_2 - w_1}{\rho_{varnish}}}$$

where w_1: weight of sample in air without varnish; w_2: weight of sample in air with varnish; w_3: weight of varnished sample immersed in water; ρ_{water}: density of deionized water; $\rho_{varnish}$: density of varnish. Measurements were performed by triplicate.

The relative density values of the sintered parts were calculated considering the theoretical density or true density as determined by helium pycnometer of grinded powders (Micromeritics AccuPyc 1330).

Shrinkage of samples was estimated by measuring samples dimensions before and after sintering. For each type of sample, the measurements were obtained by quintupled.

2.2.6. Ionic conductivity measurements

Conductivity measurements were performed in an Impedance/Gain-Phase Analyzer SI1260 (Solartron, UK). Impedance tests were carried out by applying a 100 mV amplitude signal in the 0.1 Hz - 1 MHz frequency range. Prior to impedance measurements, gold blocking electrodes were painted on both sides of the pellets and fired at 800 °C for an hour. Measurements were performed on porous samples with and without ionic liquids. For comparison purposes, a pore-free sample without ionic liquid was also analyzed. To avoid any moisture contact, all cells were assembled in a glove box with argon atmosphere. Measurements at different temperatures (from -30 °C to +90 °C) were carried out. To obtain reproducible measurements, we established a dwell time of 30 min before taking every measurement, in order to reach a stable temperature. The dc conductivity values were obtained from the complex impedance plot (Z''*vs* Z') by determining the intersection point of the real axis with the spike formed at the end of the semicircle.

2.2.7. Electrochemical performances

Na$^+$ insertion/extraction was evaluated by galvanostatic charge-discharge (GCD) tests in two-electrode coin cells (CR2032). Cycling tests were performed with a Neware BTS-4000 battery tester at different c-rates in the potential range from 3–3.8 V at room temperature.

3. Results

3.1. Effect of Na concentration and sintering temperature

For optimization purposes, the effect of sodium concentration and heating temperature on sintering was studied for non-porous samples. Fig. S1 shows the XRD patterns, recorded at room temperature, for bare and Na-excess samples (10 % and 20 % Na-excess) sintered at different temperatures. These patterns confirm the existence of single phases for all the samples, except for the bare sample sintered at the lowest temperature (1100 °C), where only a non-identified extra peak appears at 2θ≈ 29 °. Unlike the results found by Park et al. [30], in similar samples with Na-excess, no extra peaks associated with Na$_3$PO$_4$ appear in the XRD patterns, even for the sample with the highest sodium concentration (20 % Na-excess). Regarding structural features of the synthesized samples, most adopt a monoclinic symmetry. However, for the highest sintering temperature (1200 °C) and for both samples with Na-excess, some evidence of a rhombohedral symmetry appears (see supplementary information).

Fig. 1 displays the microstructure obtained for bare samples (0% Na-excess) sintered at different temperatures: 1100 °C, 1150 °C and 1200 °C. At the lowest sintering temperature, the microstructure presents high porosity and small particles (<1 μm) of irregular morphology, characteristic of the first stage of the sintering process. As temperature increases, as expected, porosity decreases and particles are more rounded. For the highest sintering temperature (1200 °C), there is a slight grain growth and greater densification of the sample. Regarding
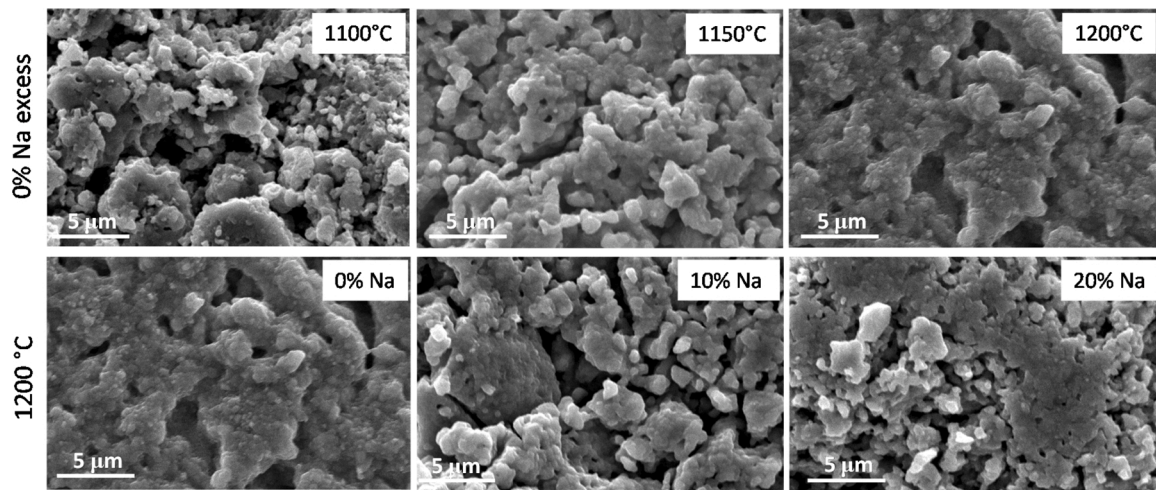
Fig. 1. SEM images of samples sintered under different conditions showing the influence of %Na excess and sintering temperature on the material microstructure. Top row: 0%Na excess at different sintering temperatures. Bottom row: different %Na excess at a sintering temperature of 1200 °C.

the effect of sodium concentration, Fig. 1 also shows the microstructure of samples with different extra-Na content sintered at 1200 °C. As observed, the Na-excess does not promote the sintering process, on the contrary, as sodium concentration increases, porosity and defects appear on the surface, affecting the densification of the samples, and, therefore, subsequent mechanical properties. Park et al. [30] reported the influence of Na concentration, where unlike our observations, no significant variations in microstructure were detected. This could be explained by the slight difference in NASICON composition (cubic YSZ was used as precursor, instead of monoclinic ZrO_2) and by the sintering procedure used.

It is well known the volatilization of Na_2O, even P_2O_5, during sintering of NASICON at high temperatures, producing the segregation of zirconia at the grain boundary, which provokes a decrease in the ionic conductivity [47]. Bohnke et al. [48] reported that the presence of

zirconia as a second phase could be associated to a deficiency of Zr in NASICON, which could be detrimental for ionic conductivity. To determine possible sodium and/or phosphorus losses at the pellets surface during the sintering process, the cross-sectional area of samples was studied by using X-ray mapping. As shown in Fig. 2, all samples present a homogeneous distribution of both elements (Na and P), no matter sintering temperature nor sodium concentration. Small black regions refer to inherent porosity derived from the processing methodology.

The absence of eventually secondary phases, also verified by XRD (Fig. S1 in the supporting information), confirms that P and Na volatilization is avoided. This could be ascribed to the use of extra powder material covering samples and to the low heating rates applied during the thermal treatments.

Regarding volumetric contraction after sintering, as shown in Fig. 3A, a significant increase in densification was observed for bare
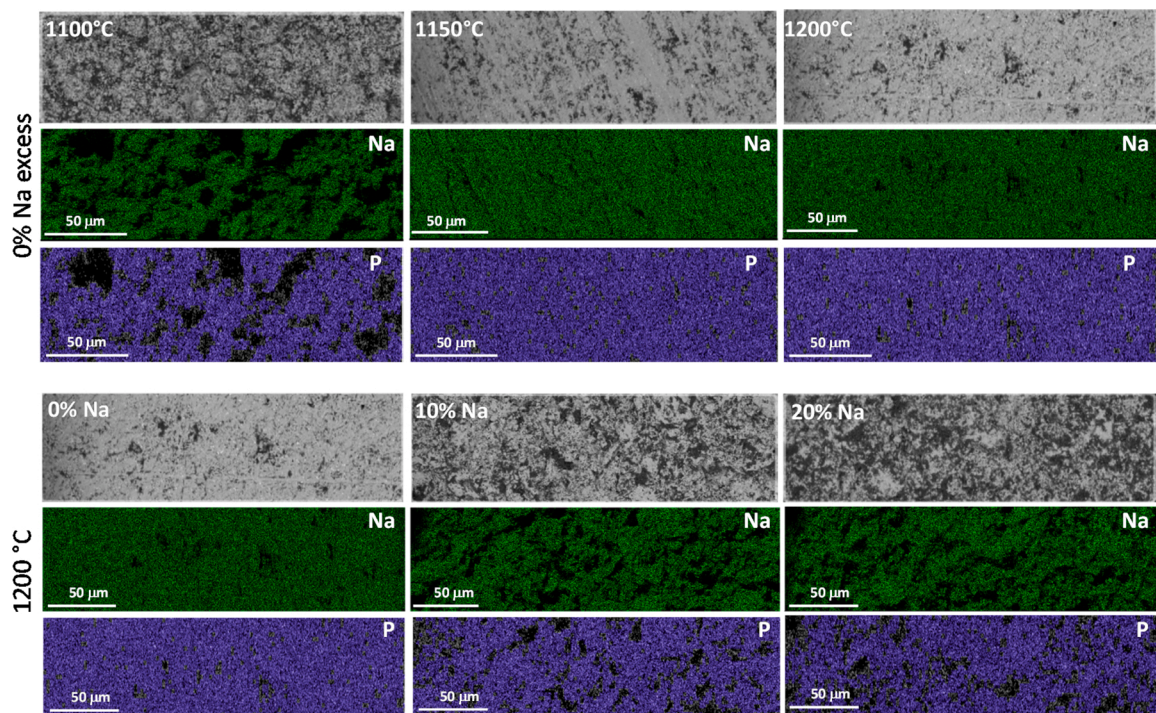

Fig. 2. SEM images and mapping corresponding to Na and P distribution through the cross-sectional area for samples with different Na content sintered at 1200 °C (bottom) and with 0% extra Na sintered at different temperatures (top).
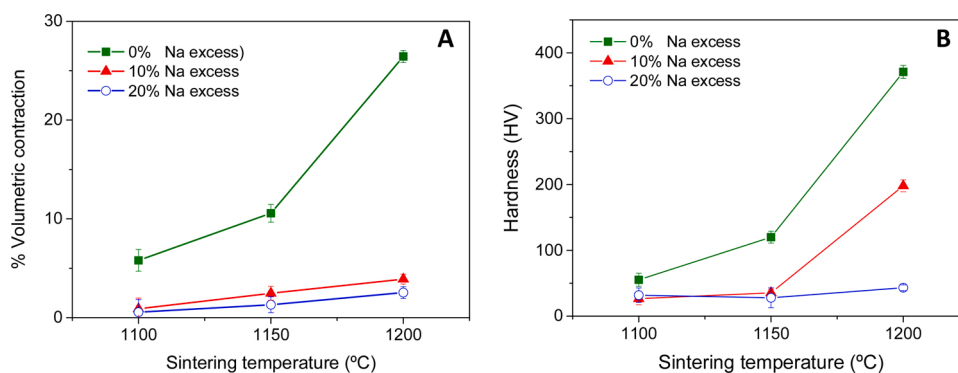
Fig. 3. Influence of %Na and sintering temperature on (A) volumetric contraction (densification) and (B) microhardness (Vickers).

samples (without Na-excess) as sintering temperature increased, with a maximum of 25 % at 1200 °C. However, samples with 10 % and 20 % of Na-excess presented only a negligible effect in shrinkage (less than 3 %) according to the sintering temperature. This fact agrees with the micrographs obtained by SEM (see Fig. 1), where a lack of sintering was observed as sodium concentration was increased.

To evaluate the effect of sintering temperature and sodium concentration on mechanical properties, Vickers microhardness was measured for all samples. To obtain reproducible values, ten measurements were taken at different points on each sample surface. According to Vickers microhardness (see Fig. 3B), an increase in sodium content is detrimental to hardness. This agrees with the microstructure observed by SEM, since higher porosity and more disconnected particles are more likely as sodium concentration increases. On the other hand, higher temperature favors the sintering process and, consequently, the densification of the samples, enhancing hardness of the material for all sodium concentrations.

Regarding ionic conductivity, impedance measurements were performed for samples with different sodium excess (0 %Na, 10 %Na, 20 % Na) and sintering temperatures (1100 °C, 1150 °C, 1200 °C) as a function of temperature, while heating, in the range from −30 °C to 90 °C. According to these measurements, best conductivity values were found for samples 0 %Na-excess sintered at 1200 °C (see Fig. S2 in supplementary information), reaching values of 0.24 mS cm^{-1} and 0.45 mS cm^{-1} and at 30 °C and 50 °C, respectively; values slightly lower than those previously reported for denser samples [31]. This fact evidences the importance to achieve a well-sintered ceramic to reach good values of total conductivity [49].

According to results obtained regarding sintering temperature and sodium concentration, porous samples were prepared from the stoichiometric amount of the desired phases (without Na-excess) and sintered at 1200 °C. As previously mentioned, two approaches were tried to obtain porous samples: using organic materials as pore-formers and applying freeze-casting.

3.2. Porous samples prepared with pore-formers

Powder of NASICON 0 %Na-excess was used to produce porous pellets to be subsequently infiltrated with ionic liquids, towards the attainment of hybrid sodium electrolytes. For this purpose, different pore formers were used: rice starch, cornstarch, potato maltodextrin and PMMA. The use of cheap, simple and accessible pore formers offers a huge potential for developing porous ceramics with controlled pore size, morphology and distribution [50]. It is expected that the type, shape and content of pore-formers produce variations not only in the samples microstructure, but also in their transport properties and, consequently, in their electrochemical behavior. Disks of 13 mm diameter and approximately 1.5 mm thickness were obtained by uniaxial pressing compaction, applying 220 MPa during 5 min. To evaluate the effect of the pore-former amount, they were added in two volumetric ratios, 10 %

and 20 %. The optimized thermal cycle applied to each sample is depicted in Fig. S4. The first step of the thermal cycle corresponds to the elimination/degradation of the pore-former and it was specifically designed on the basis of thermogravimetric analysis of each pore former (see Fig. S3 in supplementary information) and the former analysis of bare NASICON powder.

3.2.1. Study of microstructure

The elimination of the corresponding pore-former produces different microstructures, since not only the volume fraction, but also the particle size and morphology are key factors. According to SEM images, provided in Fig. S5 in supporting information, all pore-formers, except PMMA (spheres 50–100 μm diameter), are irregular in shape, being those of rice starch the smallest ones (~ 10 μm) and those of potato maltodextrin the ones with the broadest particle size distribution. In addition, given the high hygroscopicity of rice starch, particles tend to form agglomerates.

Fig. S6 in the supporting information shows the microstructure obtained for samples 10 vol.% fraction of pore formers. Independently of the pore formers used, the higher the volume fraction of pore-former, the higher the achieved porosity. Fig. 4 displays SEM images of the samples surface showing porosity achieved for a 20 vol.% of pore former. PMMA produces large pores that give rise to cracks in the microstructure, which would be detrimental for mechanical properties. In the case of samples obtained by using potato maltodextrin, a non-uniform pore size distribution is observed, when compared with the rest of samples, with zones with large pores joined to surface cracks. The most uniform pore distribution is obtained for cornstarch, followed by rice starch. However, samples consolidated with rice starch present some regions with larger pores. This could be associated to the trend of rice starch to form agglomerates. These results suggest that the pore formers behave as templates, by printing their morphology in the resulting microstructure. Hence, the pore former can be used to control the pore size and shape in the final microstructure of the sintered compact. Shen et al. [51] reported the use of polystyrene (PS) with different particle diameter (83, 200, 300, 400 and 500 μm) as a pore former in sintered diatomite ceramics to demonstrate the influence of particle size and amount of pore former in the achieved porosity. Nevertheless, in the case of samples obtained by using PMMA as pore former, despite pores with spherical morphologies were expected, the milling process probably modified the spherical particles (deforming and/or fracturing), producing mainly irregular shapes. Therefore, not only the size and morphology of pore formers but also processing techniques influence the final microstructure [52].

Fig. 5 shows the influence of vol.% of cornstarch on sample porosity, when compared to bare samples. SEM images correspond to samples surface. According to these images, porosity increases as vol.% of cornstarch increases. In addition, as seen in zoom in images, a uniform distribution of porosity is achieved for both volume fractions. Such influence of the volume fraction of the pore former used has been reported
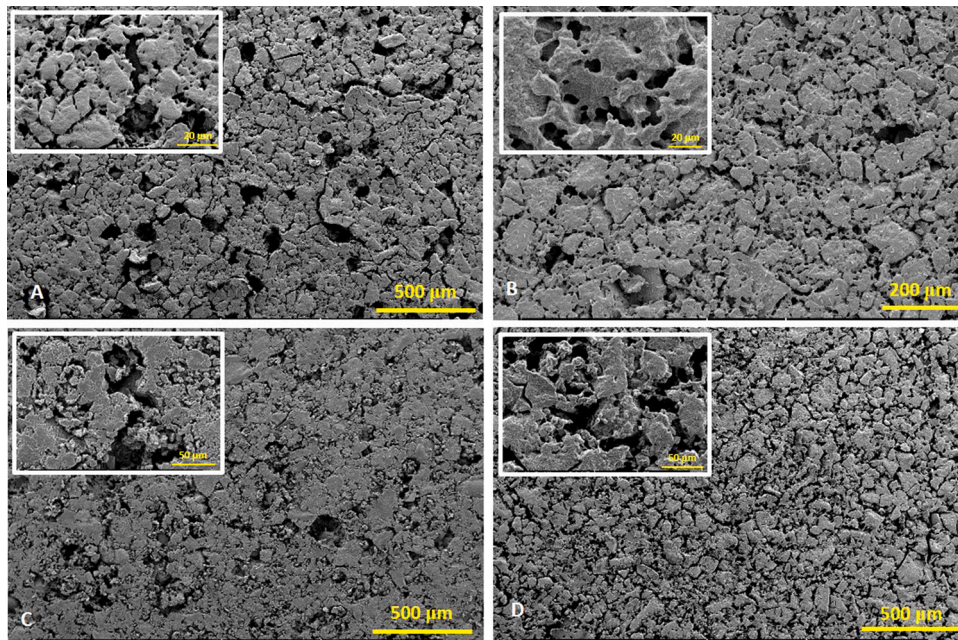
Fig. 4. Porosity pattern obtained for each pore former at a 20 vol. % A: PMMA; B: rice starch; C: potato maltodextrin; D: cornstarch.
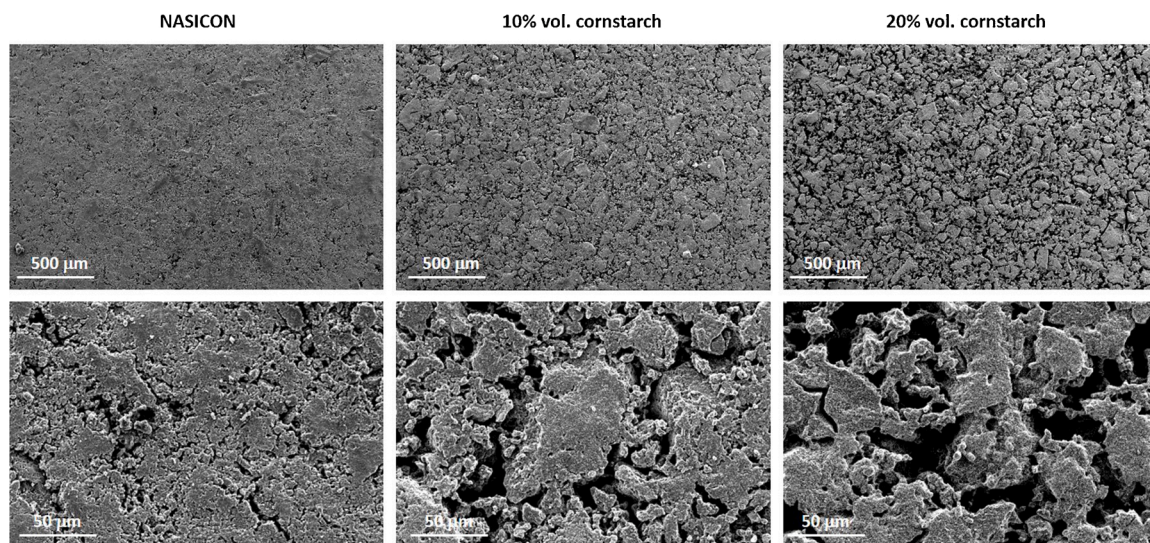

Fig. 5. Effect of vol.% of cornstarch on sample porosity.

for YSZ wafers when using graphite and PMMA [53].

3.2.2. Densification of porous samples

Density of porous samples was characterized by helium pycnometry (true density) and the Archimedes method (apparent density). According to Fig. 6, all samples presented higher true density as compared to apparent density, with no significant differences between the different porous samples. This is in agreement with the fact that true density should approach that of the non-consolidated powders, 3.24 g/cm^3($\pm$0.02). Regarding apparent density, no significant differences were observed between cornstarch, potato maltodextrin and rice starch. However, PMMA presented the lowest values. This could be associated to the larger pore size, which could be detrimental for the sintering process, limiting densification. According to true and apparent density, open, closed and total porosity was estimated (Fig. 6-b), being the total porosity of the different samples 17.3 % (cornstarch), 17.0 % (potato maltodextrin), 25.0 % (PMMA) and 17.9 % (rice starch).

3.2.3. Infiltration with ionic liquids

To promote ionic conductivity at room temperature, porous samples were infiltrated with a solution 10 % NaTFSI in commercial 1-Butyl-1-Methylpyrrolidium bis(trifluoromethanesulfonyl)amide (Pyr0408a). Hence, to assure a proper infiltration, wettability has been studied by contact angle measurements. In samples with high porosity, infiltration is a dynamic process, therefore, the initial characterization consisted on measuring the time elapsed for a drop of ionic liquid (IL)-NaTFSI, with a specific volume, to be completely absorbed. For this purpose, drops 1.5 µl were dispensed on the pellets surface for all samples. To promote reproducibility, measurements were performed by triplicate for each porous sample type. Fig. 7 shows the absorption rate, calculated as the drop volume divided by the absorption time, for all samples. As expected, all samples presented improved absorption rates when compared to the pore-free sample. Furthermore, the absorption rate improves considerably with the level of porosity using the same pore-former. The fastest absorption occurred for cornstarch-based samples,
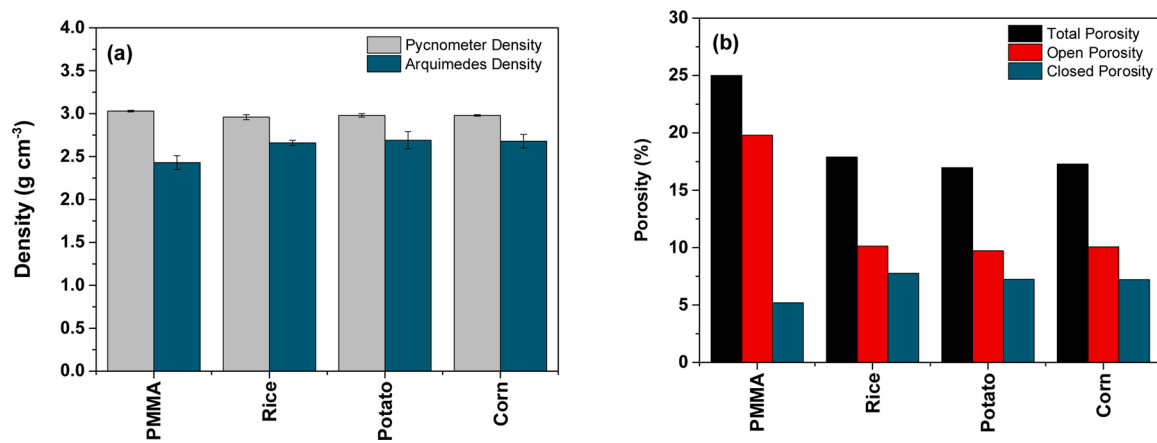
Fig. 6. Comparison of (a) density and (b) porosity (open, closed and total) for porous compacted samples obtained from the use of pore formers at a 20 vol.%.
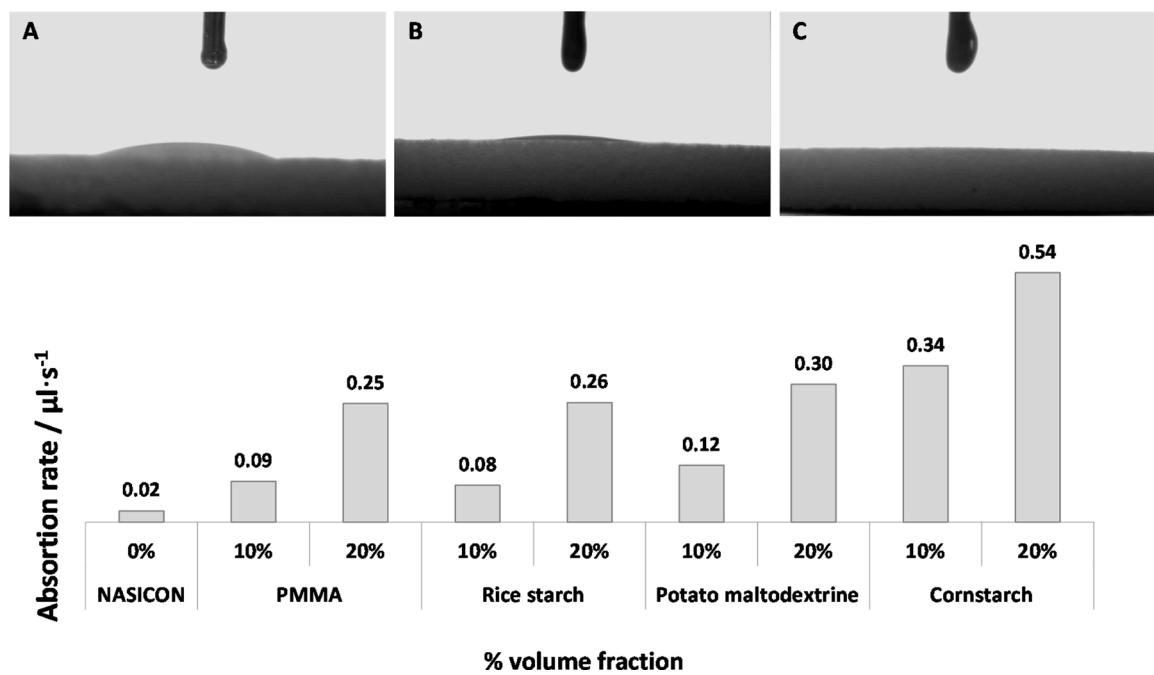

Fig. 7. Top: images of the drop obtained after 3 s of ionic liquid deposition (A: NASICON; B: 10 vol.% cornstarch; C: 20 vol.% cornstarch). Bottom: absorption rate for porous samples obtained with different pore formers and at different volume fraction.

in particular those of 20 vol.%, 0.54 µl/s (3 s), despite having smaller pores and apparently higher density. It is worth to mention that the second best result was achieved by the sample of 10 vol.% cornstarch, which could mean that the influence of the pore-former type is more relevant than the volume fraction of the pore-former. This could be linked to the uniformity of particle size and distribution of pores obtained when using this material, as explained above.

By using three seconds as reference time (time required for a complete absorption for the fastest sample: 20 wt.% cornstarch), contact angles were measured for all samples. Table 2 summarizes results obtained. As expected, lower contact angles were obtained as the volume fraction increased from 10 % to 20 % for all cases. Moreover, as previously stated, best results, regarding wettability were obtained for porous samples produced by using cornstarch as pore-former.

3.3. Porous samples prepared by freeze-casting

NASICON powders without Na excess were used to produce aqueous slurries with different powder volume fractions: 30 %, 40 % and 50 %.

Table 2
Contact angle measurements for porous samples based on different pore former and volume fraction.

Pore former	Vol.%	Contact angle (°)
NASICON	0 %	22.1 ± 5.4
Rice starch	10 %	11.6 ± 0.2
	20 %	7.5 ± 0.9
Cornstarch	10 %	3.9 ± 0.9
	20 %	–
Potato maltodextrin	10 %	11.0 ± 2.8
	20 %	7.4 ± 2.2
PMMA	10 %	17.2 ± 4.1
	20 %	7.9 ± 1.9

These powder loading were selected on the basis of previous works reported for TiO_2 [54] and alumina [55,56]. As explained in experimental section, these aqueous slurries were frozen, lyophilized and finally heated at the optimized sintering temperature.

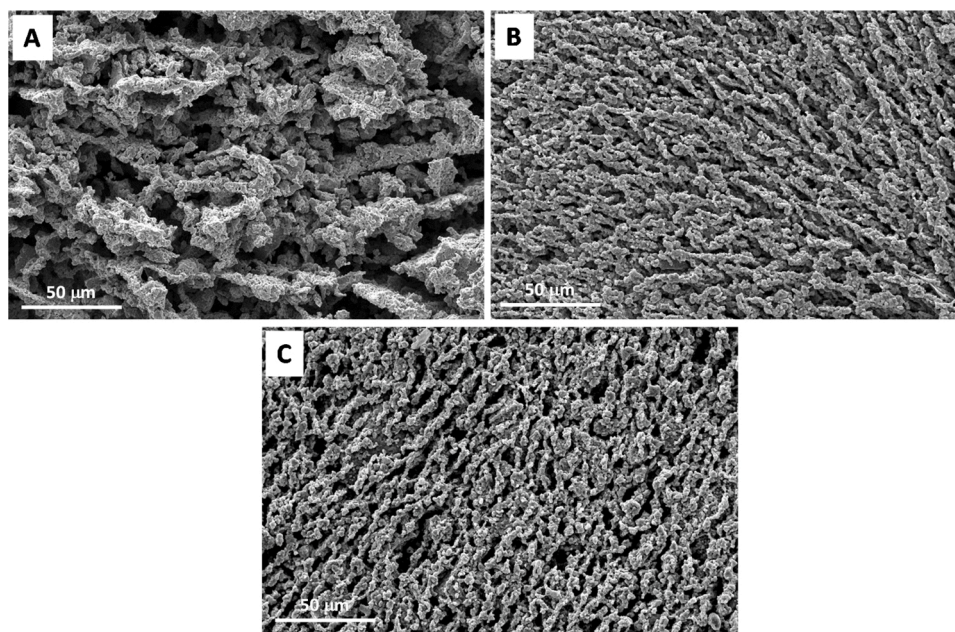Fig. 8 presents the top view of sintered samples. According to SEM

Fig. 8. Top view of porous samples obtained by freeze-casting. **A:** 30 vol.% NASICON; **B:** 40 vol.% NASICON; **C:** 50 vol.% NASICON.

images, as expected, porosity increases as the volume fraction of NASICON decreases, being that for sample 30 % volume fraction the one with the highest porosity level. The morphology of the porous samples obtained is highly different when compared with that previously obtained for samples processed by using pore-formers as sacrificial materials. The porosity obtained is a replica of the ice crystals, given the sublimation produced during the lyophilization process. In general, images exhibit pores with an elongated morphology, with higher connectivity as powder load increases. It was found that the pore channels became narrower as the solid content increased. Columnar channels are aligned along the ice growth direction and distributed homogeneously through the sample. Indeed, the addition of PVA serves two purposes, as binder to enhance mechanical properties of green pieces and as a way to control the pore structure during the freezing procedure [57]. The addition of the PVA aqueous solution into the slurries affects the final solid content and, therefore, the porosity degree. As the PVA solution concentration increases, pores loss directionality (see Fig. 8A), presenting instead a more equiaxed distribution without identifiable orientation. According to Wang et al., the growth of ice crystals is hindered by a phase of ceramic walls formed by ceramic particles surrounded by PVA. As the PVA concentration increases, a higher resistance for crystals growth arises, which results in a non-oriented porous structure [57], as shown in Fig. 8A.

In this case, given the high degree of porosity, contact angle measurements were not possible, since the ionic liquid was instantaneously absorbed when contact with the surface was achieved, suggesting an excellent wettability.

3.4. Ionic conductivity

The trend of total ionic conductivity as a function of temperature during heating is reported in Fig. 9 for all hybrid electrolytes. Conductivity data of the two components of the hybrid electrolyte, a non-porous NASICON sample and the ionic liquid/NaTFSI solution, were also included for comparison purposes. In a first view, it can be seen that all hybrid electrolytes present similar conductivities among them with values ranging between those of the two components used separately throughout the whole temperature range.

Regarding samples obtained by using pore formers, in a more detailed analysis, only negligible differences were observed when comparing them. The highest ionic conductivity was achieved at 90 °C for PMMA-based samples (20 vol.% PMMA), reaching 5.8 mS cm^{-1}, one order of magnitude higher compared to the pore-free sample. Conductivity values at room temperature are depicted in Table 3.

Regarding samples obtained by freeze-casting (Fig. 9 - right), in general terms, conductivity increases as porosity does. This probably responds to their improved capability to host liquid inside. The highest ionic conductivity was achieved at 90 °C for the 30 vol. % NASICON sample, reaching 4 mS cm^{-1}.

Despite freeze-casting samples present higher porosity than those obtained by using pore-formers, they exhibited slightly lower ionic conductivity values. This could be related to the geometry and size of the porosity obtained by freeze-casting, which, for some reason, limits the liquid accommodation within the porous inorganic macrostructure. This fact impedes to achieve the percolation threshold. The microstructure of freeze-casting samples is based on columnar pores perpendicularly oriented regarding the ions path, which may hinder ionic conductivity. This is not the case for porous samples obtained by using pore-formers, since a more uniform porosity path through their cross-sectional area was achieved.

The temperature dependence of the conductivity of all hybrid electrolytes and the ILs follows the Vogel-Tamman-Fulcher (VTF) behavior,

Table 3

Ionic conductivity at room temperature, MacMullin number (N_M) and VTF parameters obtained for all hybrid electrolytes, where A is the pre-exponential factor, T_0 is a parameter correlated to the glass transition temperature and B is the pseudo-activation energy.

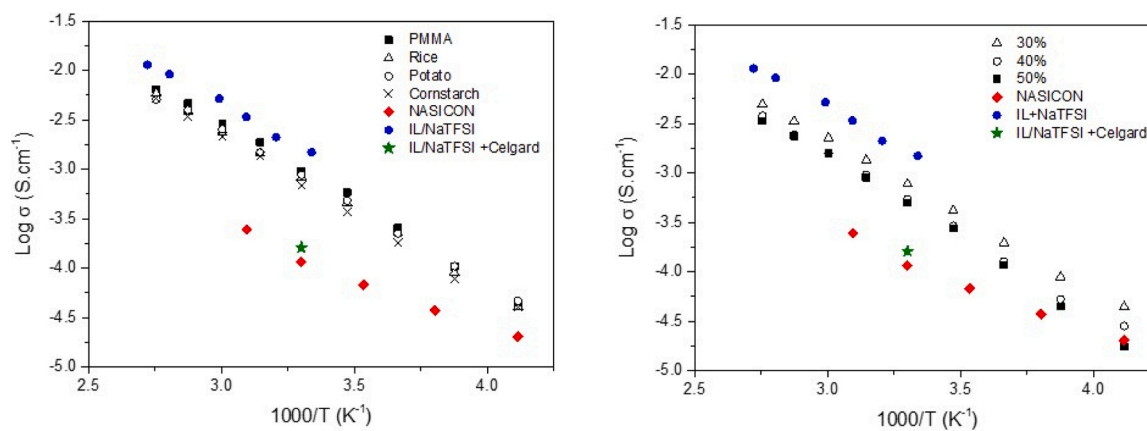|	T_0 (K)	A	B (eV)	σ (S cm^{-1}) @ 30 °C	N_M @ 30 °C
IL/NaTFSI solution	89.9	7.9	0.16	1.5×10^{-3}	–
20 vol.% PMMA	78.7	4.7	0.16	9.6×10^{-4}	1.5
20 vol.% potato maltodextrine	64.1	6.7	0.19	8.7×10^{-4}	1.7
20 vol.% rice starch	91.7	3.3	0.15	8.2×10^{-4}	1.8
20 vol.% cornstarch	72.7	5.9	0.18	6.8×10^{-4}	2.2
Freeze-casting (30 %)	103.5	2.0	0.14	5.6×10^{-4}	2.6
Freeze-casting (40 %)	89.1	3.5	0.16	5.3×10^{-4}	2.8
Freeze-casting (50 %)	77.1	5.4	0.17	4.8×10^{-4}	3.1
IL/NaTFSI solution + Celgard2325	–	–	–	1.3×10^{-4}	11.6

Fig. 9. Conductivity measured at different temperatures for hybrid electrolytes. Left: samples prepared with different pore formers. Right: samples obtained by freeze-casting. Ionic conductivity of a non-infiltrated porous-free sample, the infiltrating solution [40], and a Celgard 2325® + infiltrating solution (labelled as green star) are also plotted (For interpretation of the references to colour in this figure legend, the reader is referred to the web version of this article).
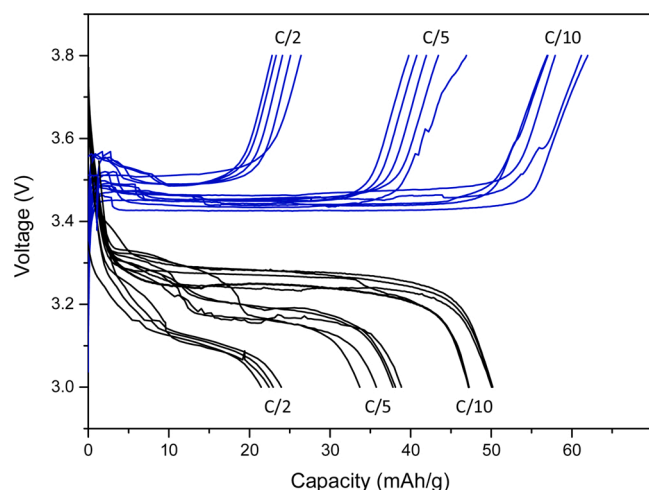

Fig. 10. Galvanostatic charge-discharge profiles of NVPC cathode at different C-rates when using NASICON 20 vol.% cornstarch + IL as quasi-solid state electrolyte.

a widely used approximation for non-Arrhenius polymeric ion conductors:

$$\sigma = A \bullet e^{-\frac{B}{K(T-T_0)}}$$

Where σ is the ionic conductivity, A is the pre-exponential factor, T_0 is a parameter correlated to the glass transition temperature (T_g) and B is the pseudo-activation energy. The fitting results (curves and data) are depicted in Figs. S7 and S8 of Supplementary Information.

In general terms, hybrid electrolytes present basically the same activation energy than the IL.

According to results obtained, conductivity is improved for all samples once they are infiltrated with the IL/NaTFSI solution. This could be ascribed to the effect of the ionic liquid reducing the grain boundary resistance in the ceramic solid electrolyte particles through the HSE, which facilitates the diffusion of Na^+ ions through the NASICON-IL interface [58]. On the other hand, the fact that all samples exhibit a non-Arrhenius behavior, together with the fact that all of them exhibit an intermediate conductivity between that of the ionic liquid and that of pore-free NASICON, suggests that, conductivity is governed by the ionic liquid and, for some reason, the percolation threshold has not been reached. However, since both activation energy and T_0 values change for all samples, it could be inferred that some kind of interaction, albeit small, between the ionic liquid and the inorganic solid exists.

Moreover, in IL-free NASICON the porosity is filled by air; while in the IL-filled NASICON this porosity is filled by the IL/NaTFSI solution, whose conductivity is very high. Hence, the porous NASICON might be considered as a functional macroporous inorganic separator that can act as a Na^+ reservoir, improving the ionic conductivity. In fact, a commercial porous Celgard 2325 separator infiltrated with the Na-ILs solution presented an ionic conductivity (0.13 mS cm^{-1} at 30 °C) lower than any of the hybrid electrolytes proposed. Table 3 summarizes MacMullin numbers (N_M) obtained for all HSE electrolytes compared with Celgard 2325®. The N_M reflects the efficiency of a battery separator since it is a representation of the increase in resistivity when coupled to a free electrolyte. Indeed, all HSE presented a significantly improved behavior compared to Celgard 2325®, which, according to Fig. 9, demonstrates a lack of compatibility with the high polarity exhibited by ionic liquids.

3.5. Electrochemical performance

As a preliminary evaluation of the proposed hybrid electrolytes, the electrochemical performance was tested for the optimized hybrid electrolyte: NASICON 20 % vol.% cornstarch (≈1 mm thickness) infiltrated with the ionic liquid solution. For this purpose, Na° and NVPC ($Na_3V_2(PO_4)_3$) were used as anode and cathode, respectively, in a coin cell configuration. Fig. 10 shows charge/discharge curves of the NVPC electrode at C/10 (1 Na in 10 h), C/5 (1 Na in 5 h) and C/2 (1 Na in 2 h). In these conditions, a maximum charge capacity in the range of 61.5 mA h g^{-1} (C/10) was reached at room temperature with a Coulombic efficiency of 81.7 %. As the c-rate increases, the polarization effect becomes more significant and capacity drops to 42 mA h g^{-1} and 24 mA h g^{-1} for C/5 and C/2, respectively. Further studies are underworking in order to optimize the performance of the quasi-solid state battery in order to increase its capacity and stability at room temperature.

4. Conclusions

Hybrid quasi-solid sodium electrolytes have been successfully developed by combining porous NASICON layers with ionic liquids. In a first step, the synthesis of $Na_3Zr_{1.84}Y_{0.16}Si_2PO_{12}$ has been performed and the effect of Na-excess and sintering temperature were evaluated. According to XRD analysis, a single monoclinic phase is observed and, unlike previous publications, no extra peaks associated with Na_3PO_4 were detected for those samples with Na-excess. However, as temperature increases and sodium concentration increases, some evidence of rhombohedral symmetry was observed. Na-excess does not promote sintering and the use of YSZ as starting reagent confirmed that

substitution of Zr by Y prevents grain growth during sintering. In addition, the methodology used to prepare samples avoided loss, by volatilization during sintering, of sodium and phosphorus, since a homogeneous distribution throughout the cross section was observed.

On the other hand, NASICON porous samples have been successfully prepared by using cheap, simple and accessible pore formers. This is a significant asset, since natural, economic and environmentally friendly compounds (rice starch, cornstarch and potato maltodextrin) offers a huge potential for developing porous NASICON with controlled pore size, morphology and distribution. On the other hand, by using freeze casting, highly porous samples with directional porosity can be also obtained. The influence of microstructure has been tested in terms of wettability, hardness and ionic conductivity. After infiltration with the IL/NaTFSI solution, a significant increase in ionic conductivity has been observed, enhanced by one order of magnitude. Furthermore, the T_0 of all samples is lower than that of the IL/NaTFSI solution. This suggests that some interactions between the IL/NaTFSI solution and the inorganic solid take place, improving the grain-boundary resistance in NASICON sintered ceramic. The highest conductivity regarding hybrid electrolytes was achieved for samples 20 vol.% PMMA, reaching values up to 0.9 mS cm^{-1} at 30 °C. This demonstrates the positive effect of small amounts of ionic liquids in the transport properties of these hybrid solid state electrolytes, towards safer and environmentally friendly sodium solid state batteries.

The manufacture of thinner films of this porous NASICON would permit the manufacture of functional macroporous inorganic separators that can act as a Na$^+$ reservoirs. Despite the high thickness of the electrolyte tested, preliminary electrochemical tests are very promising.

Declaration of Competing Interest

The authors declare that they have no known competing financial interests or personal relationships that could have appeared to influence the work reported in this paper.

Acknowledgments

Appendix A. Supplementary data

Supplementary material related to this article can be found, in the online version, at doi:https://doi.org/10.1016/j.jeurceramsoc.2021.08.001.

References

[1] T.M. Gür, Review of electrical energy storage technologies, materials and systems: challenges and prospects for large-scale grid storage, Energy Environ. Sci. 11 (2018) 2696–2767, https://doi.org/10.1039/c8ee01419a.
[2] F. Nadeem, S.M.S. Hussain, P.K. Tiwari, A.K. Goswami, T.S. Ustun, Comparative review of energy storage systems, their roles, and impacts on future power systems, IEEE Access 7 (2019) 4555–4585, https://doi.org/10.1109/ACCESS.2018.2888497.
[3] J. Barsukov, Y. Qian, Battery Power Management for Portable Devices, ARTECH HOUSE, 2013.
[4] N. Yabuuchi, K. Kubota, M. Dahbi, S. Komaba, Research development on sodium-ion batteries, Chem. Rev. 114 (2014) 11636–11682, https://doi.org/10.1021/cr500192f.
[5] X. Yu, A. Manthiram, Electrode-electrolyte interfaces in Lithium-Sulfur Batteries with liquid or inorganic solid electrolytes, Acc. Chem. Res. 50 (2017) 2653–2660, https://doi.org/10.1021/acs.accounts.7b00460.
[6] X. Yu, A. Manthiram, Ambient-temperature energy storage with polyvalent metal-sulfur chemistry, Small Methods 1 (2017), 1700217, https://doi.org/10.1002/smtd.201700217.
[7] M. Gauthier, A. Bélanger, P. Bouchard, B. Kapfer, S. Ricard, G. Vassort, M. Armand, J.Y. Sanchez, L. Krause, Large lithium polymer battery development the immobile solvent concept, J. Power Sources 54 (1995) 163–169, https://doi.org/10.1016/0378-7753(94)02060-G.
[8] M.E. Sotomayor, C. De Torre-gamarra, W. Bucheli, J.M. Amarilla, Additive-free Li4Ti5O12 thick electrodes for Li-ion batteries with high electrochemical performance, J. Mater. Chem. A Mater. Energy Sustain. 00 (2018) 1–10, https://doi.org/10.1039/C7TA10683A.
[9] Y. Kato, S. Shiotani, K. Morita, K. Suzuki, M. Hirayama, R. Kanno, All-Solid-State Batteries With Thick Electrode Con Fi Gurations, 2018, https://doi.org/10.1021/acs.jpclett.7b02880.
[10] C. Zhao, L. Liu, X. Qi, Y. Lu, F. Wu, J. Zhao, Y. Yu, Y.S. Hu, L. Chen, Solid-state sodium batteries, Adv. Energy Mater. 8 (2018) 14–16, https://doi.org/10.1002/aenm.201703012.
[11] J.-J. Kim, K. Yoon, I. Park, K. Kang, Progress in the development of sodium-ion solid electrolytes, Small Methods 1 (2017), 1700219, https://doi.org/10.1002/smtd.201700219.
[12] Y. Kato, S. Hori, T. Saito, K. Suzuki, M. Hirayama, A. Mitsui, M. Yonemura, H. Iba, R. Kanno, High-power all-solid-state batteries using sulfide superionic conductors, Nat. Energy. 1 (2016) 1–7, https://doi.org/10.1038/nenergy.2016.30.
[13] J. Janek, W.G. Zeier, A solid future for battery development, Nat. Energy. 1 (2016) 1–4, https://doi.org/10.1038/nenergy.2016.141.
[14] C. Zhou, S. Bag, V. Thangadurai, Engineering materials for progressive all-solid-State Na batteries, ACS Energy Lett. 3 (2018) 2181–2198, https://doi.org/10.1021/acsenergylett.8b00948.
[15] Z. Zhang, Y. Shao, B. Lotsch, Y.S. Hu, H. Li, J. Janek, L.F. Nazar, C.W. Nan, J. Maier, M. Armand, L. Chen, New horizons for inorganic solid state ion conductors, Energy Environ. Sci. 11 (2018) 1945–1976, https://doi.org/10.1039/c8ee01053f.
[16] K.B. Hueso, M. Armand, T. Rojo, High temperature sodium batteries: status, challenges and future trends, Energy Environ. Sci. 6 (2013) 734–749, https://doi.org/10.1039/c3ee24086j.
[17] J.B. Goodenough, H.Y. Hong, J.A. Kafalas, J.B. Goodenough, H. Y-P, Mater. Res. Bull. 11 (1976) 203–220.
[18] H.Y.P. Hong, Crystal structures and crystal chemistry in the system Na1+xZr2SixP3-xO12, Mater. Res. Bull. 11 (1976) 173–182, https://doi.org/10.1016/0025-5408(76)90073-8.
[19] Y. Shao, G. Zhong, Y. Lu, L. Liu, C. Zhao, Q. Zhang, Y.S. Hu, Y. Yang, L. Chen, A novel NASICON-based glass-ceramic composite electrolyte with enhanced Na-ion conductivity, Energy Storage Mater. 23 (2019) 514–521, https://doi.org/10.1016/j.ensm.2019.04.009.
[20] E. Wang, H.-P. Wu, C.-H. Chiu, P.-H. Chou, The effect of battery separator properties on thermal ramp, overcharge and short circuiting of rechargeable Li-Ion batteries, J. Electrochem. Soc. 166 (2019) A125–A131, https://doi.org/10.1149/2.0381902jes.
[21] Z. Jian, Y.S. Hu, X. Ji, W. Chen, NASICON-structured materials for energy storage, Adv. Mater. 29 (2017) 1–16, https://doi.org/10.1002/adma.201601925.
[22] N. Anantharamulu, K. Koteswara Rao, G. Rambabu, B. Vijaya Kumar, V. Radha, M. Vithal, A wide-ranging review on Nasicon type materials, J. Mater. Sci. 46 (2011) 2821–2837, https://doi.org/10.1007/s10853-011-5302-5.
[23] H.S.H. Kohler, Composition and conduction mechanism of the NASICON structure X-Ray diffraction study on two crystals at different temperatures, Mater. Res. Bull. 18 (1983) 1143–1152.
[24] H. Gao, S. Xin, L. Xue, J.B. Goodenough, Stabilizing a high-energy-Density rechargeable sodium battery with a solid electrolyte, Chem 4 (2018) 833–844, https://doi.org/10.1016/j.chempr.2018.01.007.
[25] S. Song, H.M. Duong, A.M. Korsunsky, N. Hu, L. Lu, A Na+ superionic conductor for room-temperature sodium batteries, Sci. Rep. 6 (2016) 1–10, https://doi.org/10.1038/srep32330.
[26] F. Lalère, J.B. Leriche, M. Courty, S. Boulineau, V. Viallet, C. Masquelier, V. Seznec, An all-solid state NASICON sodium battery operating at 200°C, J. Power Sources 247 (2014) 975–980, https://doi.org/10.1016/j.jpowsour.2013.09.051.
[27] Y. Benabed, M. Rioux, S. Rousselot, G. Hautier, Assessing the electrochemical stability window of NASICON-Type solid electrolytes, Front. Energy Res. 9 (2021) 1–13, https://doi.org/10.3389/fenrg.2021.682008.
[28] H. Lee, M. Yanilmaz, O. Toprakci, K. Fu, X. Zhang, A review of recent developments in membrane separators for rechargeable lithium-ion batteries, Energy Environ. Sci. 7 (2014) 3857–3886, https://doi.org/10.1039/c4ee01432d.
[29] X. Wang, Z. Liu, Y. Tang, J. Chen, D. Wang, Z. Mao, Low temperature and rapid microwave sintering of Na3Zr2Si2PO12 solid electrolytes for Na-Ion batteries, J. Power Sources 481 (2021), 228924, https://doi.org/10.1016/j.jpowsour.2020.228924.
[30] H. Park, K. Jung, M. Nezafati, C.S. Kim, B. Kang, Sodium ion diffusion in Nasicon (Na3Zr2Si2PO12) solid electrolytes: effects of excess sodium, ACS Appl. Mater. Interfaces 8 (2016) 27814–27824, https://doi.org/10.1021/acsami.6b09992.
[31] S. Narayanan, S. Reid, S. Butler, V. Thangadurai, Sintering temperature, excess sodium, and phosphorous dependencies on morphology and ionic conductivity of NASICON Na3Zr2Si2PO12, Solid State Ion. 331 (2019) 22–29, https://doi.org/10.1016/j.ssi.2018.12.003.
[32] Q. Zhang, F. Liang, T. Qu, Y. Yao, W. Ma, Effect on ionic conductivity of Na 3 + x Zr 2-x M x Si 2 PO 12 (M = Y, La) by doping rare-earth elements effect on ionic conductivity of Na 3 + x Zr 2-x M x Si 2 PO 12 (M = Y, La) by doping rare-earth elements, IOP Conf. Ser. Mater. Sci. Eng 423 (2018), 012122, https://doi.org/10.1088/1757-899X/423/1/012122.

[33] R.O. Fuentes, F.M. Figueiredo, F.M.B. Marques, J.I. Franco, Influence of microstructure on the electrical properties of NASICON materials, Solid State Ion. 140 (2001) 173–179, https://doi.org/10.1016/S0167-2738(01)00701-9.

[34] Y. Wang, Z. Wang, J. Sun, F. Zheng, M. Kotobuki, T. Wu, K. Zeng, L. Lu, Flexible, stable, fast-ion-conducting composite electrolyte composed of nanostructured Na-super-ion-conductor framework and continuous Poly(ethylene oxide) for all-solid-state Na battery, J. Power Sources 454 (2020), https://doi.org/10.1016/j.jpowsour.2020.227949.

[35] X. Yu, J. Li, A. Manthiram, Rational design of a laminated Dual-Polymer/Polymer–Ceramic composite electrolyte for high-voltage all-solid-State Lithium batteries, ACS Mater. Lett. 2 (2020) 317–324, https://doi.org/10.1021/acsmaterialslett.9b00535.

[36] L. Chen, Y. Li, S.P. Li, L.Z. Fan, C.W. Nan, J.B. Goodenough, PEO/garnet composite electrolytes for solid-state lithium batteries: from "ceramic-in-polymer" to "polymer-in-ceramic, Nano Energy 46 (2018) 176–184, https://doi.org/10.1016/j.nanoen.2017.12.037.

[37] W. Li, S. Zhang, B. Wang, S. Gu, D. Xu, J. Wang, C. Chen, Z. Wen, Nanoporous adsorption effect on alteration of the Li+ diffusion pathway by a highly ordered porous electrolyte additive for high-rate all-solid-State Lithium metal batteries, ACS Appl. Mater. Interfaces 10 (2018) 23874–23882, https://doi.org/10.1021/acsami.8b06574.

[38] L. Long, S. Wang, M. Xiao, Y. Meng, Polymer electrolytes for lithium polymer batteries, J. Mater. Chem. A. 4 (2016) 10038–10039, https://doi.org/10.1039/c6ta02621d.

[39] S. Chen, K. Wen, J. Fan, Y. Bando, D. Golberg, Progress and future prospects of high-voltage and high-safety electrolytes in advanced lithium batteries: from liquid to solid electrolytes, J. Mater. Chem. A. 6 (2018) 11631–11663, https://doi.org/10.1039/c8ta03358g.

[40] C. de la Torre-Gamarra, G.B. Appetecchi, U. Ulissi, A. Varzi, A. Varez, S. Passerini, Na3Si2Y0.16Zr1.84PO12-ionic liquid hybrid electrolytes: An approach for realizing solid-state sodium-ion batteries? J. Power Sources 383 (2018) 157–163, https://doi.org/10.1016/j.jpowsour.2017.12.037.

[41] M. Hayyan, F.S. Mjalli, M. Ali, I.M. Alnashef, T. Xue, Journal of Industrial and Engineering Chemistry investigating the electrochemical windows of ionic liquids, J. Ind. Eng. Chem. 19 (2013) 106–112, https://doi.org/10.1016/j.jiec.2012.07.011.

[42] M. Gali, A. Lewandowski, I. St, Ionic liquids as electrolytes, Electrochim. Acta 51 (2006) 5567–5580, https://doi.org/10.1016/j.electacta.2006.03.016.

[43] L. Ren, Y. Zeng, D. Jiang, Preparation of porous TiO 2 by a novel freeze casting, Ceram. Int. 35 (2009) 1267–1270, https://doi.org/10.1016/j.ceramint.2008.04.009.

[44] F. Wang, J. Yin, D. Yao, Y. Xia, K. Zuo, Y. Zeng, Progress in Natural Science : materials International Porous SiC ceramics fabricated by quick freeze casting and solid state sintering, Prog. Nat. Sci. Mater. Int. 27 (2017) 380–384, https://doi.org/10.1016/j.pnsc.2017.04.006.

[45] R. Moreno, M.I. Nieto, K. Lebreton, J.M. Rodrı, Effect of additives on porosity of alumina materials obtained by freeze casting, Adv. Appl. Ceram. Struct. Function. Bioceram. 114 (2015), https://doi.org/10.1179/1743676115Y.0000000006.

[46] X. Liu, W. Xue, C. Shi, J. Sun, Fully interconnected porous Al 2 O 3 scaffolds prepared by a fast cooling freeze casting method, Ceram. Int. 41 (2015) 11922–11926, https://doi.org/10.1016/j.ceramint.2015.05.160.

[47] A. Ahmad, T.A. Wheat, A.K. Kuriakose, J.D. Canaday, A.G. McDonald, Dependence of the properties of Nasicons on their composition and processing, Solid State Ion. 24 (1987) 89–97, https://doi.org/10.1016/0167-2738(87)90070-1.

[48] O. Bohnke, S. Ronchetti, D. Mazza, Conductivity measurements on nasicon and nasicon-modified materials, Solid State Ion. 122 (1999) 127–136, https://doi.org/10.1016/S0167-2738(99)00062-4.

[49] J.G. Pereira da Silva, M. Bram, A.M. Laptev, J. Gonzalez-Julian, Q. Ma, F. Tietz, O. Guillon, Sintering of a sodium-based NASICON electrolyte: a comparative study between cold, field assisted and conventional sintering methods, J. Eur. Ceram. Soc. 39 (2019) 2697–2702, https://doi.org/10.1016/j.jeurceramsoc.2019.03.023.

[50] T. Dele-Afolabi, A.H. Mohamed Ariff, N. Mazlan, S. Sobri, R. Calin, I. Zahari Nur, Effect of agro-waste pore formers on the microstructure, hardness, and tensile properties of porous alumina ceramics, Int. J. Appl. Ceram. Technol. 15 (2018) 1060–1071, https://doi.org/10.1111/ijac.12874.

[51] W. Shen, L. Feng, A. Lei, Z. Liu, Y. Chen, Effects of porosity and pore size on the properties of AgO-decorated porous diatomite ceramic composites, Ceram. Int. 40 (2014) 1495–1502, https://doi.org/10.1016/j.ceramint.2013.07.034.

[52] A. Sarikaya, F. Dogan, Effect of various pore formers on the microstructural development of tape-cast porous ceramics, Ceram. Int. 39 (2013) 403–413, https://doi.org/10.1016/j.ceramint.2012.06.041.

[53] M. Boaro, J.M. Vohs, R.J. Gorte, Synthesis of highly porous yttria-stabilized zirconia by tape-casting methods, J. Am. Ceram. Soc. 86 (2003) 395–400, https://doi.org/10.1111/j.1151-2916.2003.tb03311.x.

[54] L. Ren, Y.P. Zeng, D. Jiang, Preparation of porous TiO2 by a novel freeze casting, Ceram. Int. 35 (2009) 1267–1270, https://doi.org/10.1016/j.ceramint.2008.04.009.

[55] K. Lebreton, J.M. Rodríguez-Parra, R. Moreno, M.I. Nieto, Effect of additives on porosity of alumina materials obtained by freeze casting, Adv. Appl. Ceram. 114 (2015) 296–302, https://doi.org/10.1179/1743676115Y.0000000006.

[56] C.M. Pekor, P. Kisa, I. Nettleship, Effect of polyethylene glycol on the microstructure of freeze-cast alumina, J. Am. Ceram. Soc. 91 (2008) 3185–3190, https://doi.org/10.1111/j.1551-2916.2008.02616.x.

[57] F. Wang, J. Yin, D. Yao, Y. Xia, K. Zuo, Y. Zeng, Porous SiC ceramics fabricated by quick freeze casting and solid state sintering, Prog. Nat. Sci. Mater. Int. 27 (2017) 380–384, https://doi.org/10.1016/j.pnsc.2017.04.006.

[58] H.W. Kim, P. Manikandan, Y.J. Lim, J.H. Kim, S.C. Nam, Y. Kim, Hybrid solid electrolyte with the combination of Li7La3Zr2O12 ceramic and ionic liquid for high voltage pseudo-solid-state Li-ion batteries, J. Mater. Chem. A. 4 (2016) 17025–17032, https://doi.org/10.1039/c6ta07268b.